JoTSE (2010) ISSN: 1949-4866
Volume 1, Issue 1/2, pp.

PREDICTIONS OF PERFORMANCE CHARACTERISTICS IN A LARGE TILTING PAD THRUST BEARING

D. V. Srikanth[1]* and K. K. Chaturvedi[2] and A. Chenna Kesava Reddy[3]

[1]Bharat Institute of Engineering and Technology
Mangalpally, Hyderabad , A.P., India
[2]BHEL (R&D), Vikas Nagar, Hyderabad, A.P., India
[3]JNTU Engineering College, Ananthapur, A.P., India

ABSTRACT

In the present study, formulation of the oil film shape for a flat sector-shaped bearing surface is done. The thrust segment enables change of the oil film geometry and maintains its optimum shape even with varying load. Two dimensional Reynold's equation is formulated for this bearing. Finite difference method is used to convert the Reynold's equation terms in to a set of simultaneous linear algebraic equations. A solution procedure for finding the pressure value in the oil film is described. Numerical integration of the pressure values gives the load distribution. A detailed comparison of the author's and Ettle's numerical predictions with Yuan's experimental data showed good overall agreement. Subsequently, the study of dynamic characteristics of bearing like non-dimensional stiffness and damping is done by varying the value of the oil film thickness and introducing vertical velocity in the runner.

Keywords: oil film, pressure, dynamic characteristics, finite difference methods.

NOMENCLATURE

a	:	oil film shape parameter
h	:	oil film thickness , m
h_i	:	oil film thickness at leading edge, m
h_o	:	oil film thickness at the trailing edge, m
i	:	index of the node in radial direction
j	:	index of the node in circumferential direction

* Corresponding author: dvsrikanth1@hotmail.com

m : number of the nodes on the grid in radial direction
n : number of the nodes in circumferential direction along n -axis.
p : pressure in the oil film , Pa
r_i : inner radius of the thrust pad, m
r_m : radial coordinate of the centre of pressure, m
r_o : outer radius of the thrust pad, m
r : radius of the runner, m
t : transit time ,B/U, s
A1, A2, A3: coefficients for equation of a plane
B : circumferential length of the thrust segment, m
C_z : bearing damping coefficient, N-s/m
C_z* : Non-dimensional damping coefficient
D_i : inner diameter of the thrust bearing, m
D_o : outer diameter of the thrust bearing, m
F_0, F_2, F_3 : viscosity integrals in the Reynold's equation
G_P : gap between the pads, m
H : non-dimensional thickness of the oil film, h/ho
K_z : bearing stiffness coefficient, N/m
K_z* : Non-dimensional stiffness coefficient
L : radial length of the thrust pad, m
N : angular speed of the runner, rp
P : pressure matrix in Reynold's equation
R : non - dimensional radius , r/r_o
R_{cp} : radial coordinate of the centre of pressure, m
U,V : velocity along and normal to surface, m/s
W : load on bearing, N
Z : no. of pads
γ : film thickness ratio
μ : viscosity of oil , Pa.s
θ : angle from the leading edge, radian
θ_{cp} : angular location of the centre of pressure, radian.
ρ : density of oil, kg/m3
ω : angular speed of the runner, radian /s
Δv : volume of an element of the grid , m^3
Δr : division on the grid along radial direction, m
$\Delta \theta$: angular division of the grid, radian.
ζ : coordinate along the z- axis
$\bar{\zeta}$: mean value of ζ

1. INTRODUCTION

A major component in the turbine assemblies of hydroelectric power stations is the thrust bearing. The thrust bearing carries the weight of the generator components and the hydraulic turbine plus the vertical hydraulic thrust load. The thrust load is transmitted from the rotor to

the stator through lubricant oil films that develop between a rotating collar on the shaft and the stationary sector pads in the thrust bearing. Figure 1 illustrates the geometry of the thrust pad for large thrust bearings.

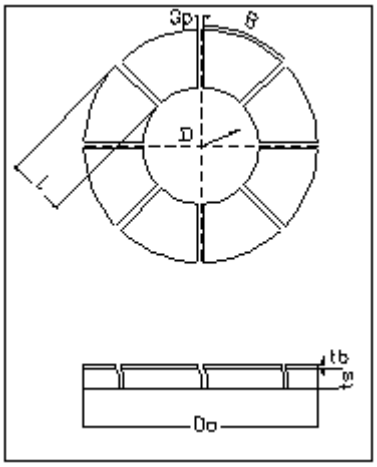

Figure 1. Geometry of the thrust pad.

The present work encompasses the first stage of research activity aimed at understanding the phenomena involved in the working of thrust bearing tilting pads. The rotor of a hydroelectric generator must move with low friction under the high load associated with its own weight and the hydraulic thrust. The bearing pads are supported by either a pivot or a distributed spring mattress. The support arrangements enable the pad to tilt and produce a lubricant film which maintains equilibrium between the generated and applied forces and moments.

Large thrust bearings in hydroelectric generators have used spring-supported sector pads as an alternative to pivot-supported pads. The application of the more complicated spring supports is common in thrust bearings with outside diameters of more than 1 m. The present study examined sector pads supported by springs as shown in figure. 2. One advantage of the distributed spring support, especially with the larger size of bearing is the ability to reduce the deflections of the pad.

An improved understanding of the hydrodynamics of the oil film and methods of calculation are essential to predict performance and design such bearings. Numerical models designing thrust bearings for the given operating conditions introduce an element of risk due to the shortage of experimental data available to check for accuracy of these predictions. Therefore there is a need, to obtain experimental data over a wide range of operating conditions and to check with the numerical model predictions. A possible approach for existing bearing designers is to obtain field data for comparison with numerical models. A full-scale apparatus to perform laboratory experiments for the simultaneous representation of thermal and mechanical influences on fluid film formation is very expensive to build and operate. The lack of an integrated theoretical and experimental investigation has made the design of thrust bearings difficult.

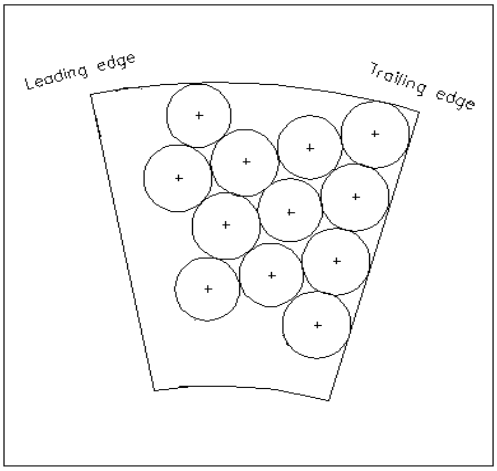

Figure 2. Spring arrangement of pad.

To develop design strategies of a large tilting pad thrust bearing there is a need for a realistic analytical model. It is essential that the predictions of this analytical model be compared with experiments that are realistic, comprehensive and allow sufficient parameter variations so as to check its fidelity. Otherwise it is almost certain that designs will be compromised by inaccuracies in the analytical model used to develop them. Therefore, the purpose of the present study is to determine the accuracy of the predictions of the present solution for large tilting pad thrust bearings by comparing it with Ettle's numerical analysis in Ettles (1991) and Yuan 's (1999) experimental data.

Vohr (1981) made the most recent attempt to perform such an analysis and include comparison with experiments for large thrust bearings. Although the agreement was good, Vohr's analysis had certain inherent approximations. Detailed checks on Vohr's analysis could not be performed without further experimental data, including pressure and oil film thickness. The agreement between experiment and theory was to be maintained over a narrow range of operating conditions. Ettle's included the thermo elastic deflection of the pad for large thrust bearings using the bi-harmonic equation for plate bending.

2. GOVERNING EQUATIONS

2.1. Shape of the Oil Film

Operation of a tilting pad thrust bearing is based on the principle of a convergent wedge formed between two surfaces moving relatively. Due to shearing action of the runner, oil is dragged into it. Reduction of the cross-sectional area squeezes oil out of the trailing and side edges. The film thickness is considered to vary in circumferential and radial directions due to the roll and pitch motion of the pad, about the centre of pressure obtained after the thrust pad is assembled. The form of the reduction of film thickness is less important than its magnitude for a wide variety of film profile forms. The variation of film thickness along and across the pad has been taken into account. The pressure in a thrust bearing is sensitive to film profile. Active face of the thrust pad is assumed flat. A flat surface has to satisfy the equation of

plane. This discrepancy was pointed out in earlier models and in Etsion (1978) a model based on the concepts of pitch line, tilt parameter and film thickness at the pivot, was proposed. Hence, the definition of the film thickness requires to be derived, from the equations of the plane. The shape of the segment is defined by its outer radius r_o, inner radius r_i, number of segments z, and the gap between the pads g_p. Other important dimensions are

$$r_m = \left[\left(r_i^2 + r_o^2\right)/2\right]^{1/2} \tag{1}$$

The angle subtended by the thrust segment at r_m is given by

$$\beta = 2\Pi/z - 2\sin^{-1}\left(g_p / 2r_m\right) \tag{2}$$

Film shape parameter for the Mitchell shape of the film is defined as:

$$a = \left(h_i - h_o\right)/h_o = \left[\left(h_i - h_o\right)/B\right]\left[B/h_o\right]$$

The film shape for a flat pad is defined by the following equation, where the oil film is convergent in positive directions of x and y axes.

$$h = A1 - A2x - A3y \tag{3}$$

for $x = r\sin\left(\theta - \theta cp\right)$ and $y = r\cos\left(\theta - \theta_{cp}\right) - r_{cp}$

The centre –of-pressure is assumed to be the origin. The coefficients A1, A2 and A3 are determined by specifying the following boundary conditions.

(a) It is seen in Figure 3 that film thickness at Q is the minimum film thickness h_o and using this boundary condition h_o in the equation (3).
(b) By using film thickness along RS and expressing γ' as the film thickness ratio in the y-direction
(c) Another boundary condition for use in the
(d) equation (3) is by considering the slope between points O and Q.
(e) Splitting γ' into two parts, one that yields uniform film thickness at the trailing edge γ_o and the other variable γ.
(f) Making film thickness to be invariant along the trailing edge.

Thus, the final form of the equation governing the shape of the oil film is given by

$$h = h_o\left[1 + \left(ar_{cp}/B\right)\tan\left(\beta - \theta_{cp}\right)\right] - h_o(ar/B)\sin\left(\theta - \theta_{cp}\right)$$

$$+h_o\left[(a/B)\tan\left(\beta-\theta_{cp}\right)-\gamma/L\right]\left[r\cos\left(\theta-\theta_{cp}\right)-r_{cp}\right] \quad (4)$$

Equation for non-dimensional thickness of the oil film is obtained by dividing both sides with h_o and is:

$$H=h/h_o=1+\left(ar_{cp}/B\right)\tan\left(\beta-\theta_{cp}\right)-(a\,r/B)\sin\left(\theta-\theta_{cp}\right)$$

$$+\left[(a/B)\tan\left(\beta-\theta_{cp}\right)-\gamma/L\right]\left[r\cos\left(\theta-\theta_{cp}\right)-r_{cp}\right] \quad (5)$$

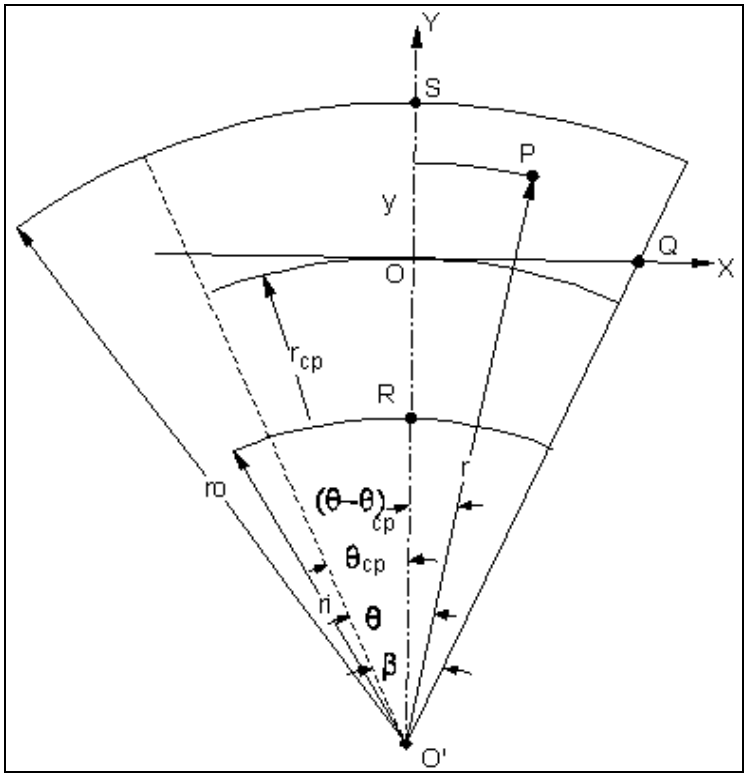

Figure 3. Shape of the oil film for a flat thrust pad.

2.2. Reynold's Equation

The analysis of hydrodynamic thrust bearings have been based on Reynold's equation for the pressure distribution. With the increasing capacity of computers numerical models including the influences of viscosity variations along and across the lubricating film have been developed. Deformation of the bearing pads due to pressure and thermal gradients were also considered.

If only the lowest order terms are retained, these can be introduced in the continuity equation which is then integrated across the fluid film to give the Reynold's equation. The temperature of the runner along its runner surface varies much less than the temperature in the thrust pad active face. The 'flash' temperature of the runner varies by less then 1^0 C and the temperature along thrust pad rises by 15 to 20 ^{0}C as in Anderson (1991). Values of viscosity obtained from the temperature field in the oil film are substituted in the Reynolds equation, to determine the pressure field. In load estimation the pressure 'fitting' at the edges has been made more appropriate to suit realistic conditions as in Chaturvedi (1989).

The generalized Reynolds equation for rectangular thrust segment is:

$$\frac{\partial}{\partial x}\left[F_2\frac{\partial p}{\partial x}\right]+\frac{\partial}{\partial y}\left[F_2\frac{\partial p}{\partial y}\right]=\frac{\partial}{\partial y}\left[\frac{F_3}{F_0}U\right] \tag{6}$$

where, $F_0=\int_0^h\frac{d\zeta}{\mu}$

$$F_2=\rho\int_0^h\frac{\zeta}{\mu}\left(\zeta-\bar{\zeta}\right)d\zeta$$

$$F_3=\rho\int_0^h\left(\zeta/\mu\right)d\zeta$$

$$\bar{\zeta}=\int_0^h\left(\zeta/\mu\right)d\zeta\Big/\int_0^h\left(d\zeta/\mu\right)$$

F_0, F_2 and F_3 are the viscosity integrals with units of m^2.sec/ kg, m .sec and sec respectively . Neglecting variation of viscosity across the thickness of the film, the Reynolds equation for a sector-shaped thrust segment for incompressible lubricant, under steady state condition is derived as in Pinkus and Sternlicht (1961) and Cameron (1966).

$$\frac{\partial}{\partial r}\left[\frac{rh^3}{\mu}\frac{\partial p}{\partial r}\right]+\frac{1}{r}\frac{\partial}{\partial\theta}\left[\frac{h^3}{\mu}\frac{\partial p}{\partial\theta}\right]=6\omega r\frac{\partial h}{\partial\theta}+12r\frac{\partial h}{\partial t} \tag{7}$$

Usual assumptions are made in the analysis done herein.

The Reynolds equation in non-dimensional form is:

$$2\frac{\partial}{\partial R}\left[\frac{RH^3}{\bar{\mu}}\right]\frac{\partial p}{\partial R}+\frac{2RH^3}{\bar{\mu}}\frac{\partial^2 P}{\partial R^2}+\frac{2}{\beta^2 R}\frac{\partial P}{\partial\bar{\theta}}\frac{\partial}{\partial\bar{\theta}}\left[\frac{H^3}{\bar{\mu}}\right]+\frac{2}{\beta^2 R}\frac{H^3}{\bar{\mu}}\frac{\partial^2 P}{\partial\bar{\theta}^2}=12R\frac{\partial H}{\partial\bar{\theta}}$$

$$+24R\ \beta\ \frac{\partial H}{\partial\bar{t}} \tag{8}$$

As compared to the above form of the equation, better numerical accuracy can be obtained, if all the first derivative terms in the equation are converted in to second derivative terms. Adopting this procedure the following equation is obtained.

$$\frac{\partial^2}{\partial R^2}\left[\frac{RH^3 p}{\bar{\mu}}\right]+\frac{RH^3}{\bar{\mu}}\frac{\partial^2 P}{\partial R^2}-P\frac{\partial^2}{\partial R^2}\left[\frac{RH^3}{\bar{\mu}}\right]+\frac{1}{R\beta^2}\frac{\partial^2}{\partial \bar{\theta}^2}\left[\frac{H^3 P}{\bar{\mu}}\right]$$

$$+\frac{1}{R\beta^2}\frac{H^3}{\bar{\mu}}\frac{\partial^2 P}{\partial \bar{\theta}^2}-\frac{P}{R\beta^2}\frac{\partial^2}{\partial \bar{\theta}^2}\left[\frac{H^3}{\bar{\mu}}\right] \tag{9}$$

$$=12R\frac{\partial H}{\partial \bar{\theta}}+24R\beta\bar{V}$$

3. COMPUTATIONAL PROCEDURE

Solution of Reynold's equation using FDM discretization of thrust pad is done by considering a total of 81 nodes in the form of a grid as shown in figure 4.

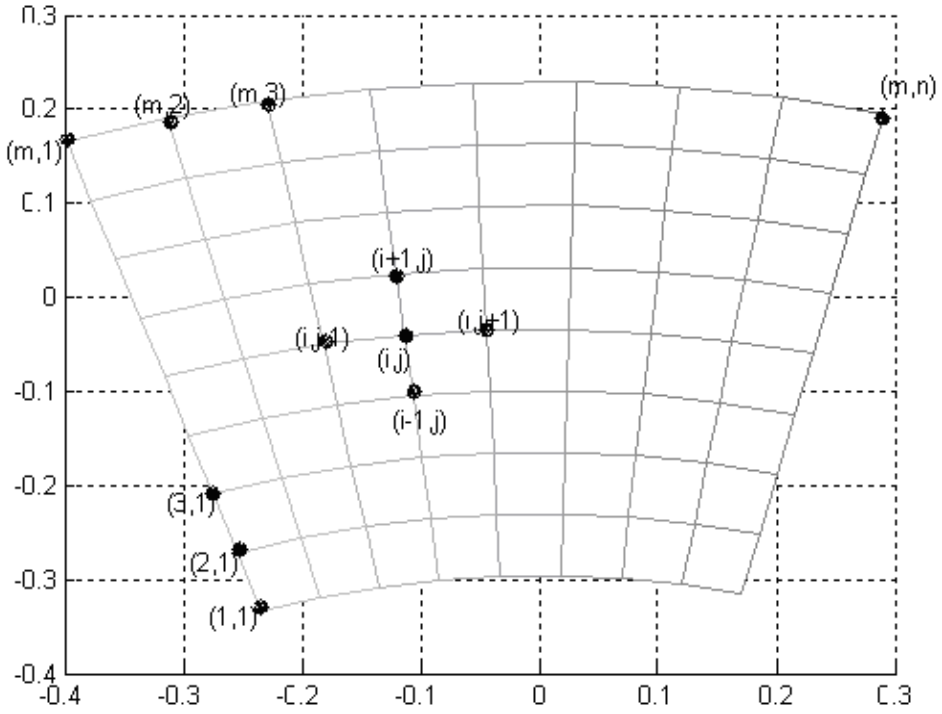

Figure 4. Discretization of pad for Reynold's equation.

The Reynold's equation is a non-homogeneous partial differential equation of two variables for which closed form analytical solutions are not available. The use of finite difference methods for a numerical approximation of this type of partial differential equation is discussed in Capitao (1974).

The Finite difference equation is derived by approximating the derivatives in the differential equation via the truncated Taylor series expansion for three successive grid points. The central difference form where in the values of the function at adjacent nodes on either side are required to evaluate the derivatives is used .Writing the Reynold's equation in the above finite difference form as in (10) results in a set of linear algebraic equations which can be transformed into matrix form and solved simultaneously by available subroutines. This yields the non-dimensional pressure at each node.

$$P_{i+1,j}\left[\frac{R_{i,j}H_{i,j}^3}{\Delta R^2\overline{\mu}_{i,j}}+\frac{R_{i+1,j}H_{i+1,j}^3}{\overline{\mu}_{i+1,j}\Delta R^2}\right]+P_{i-1,j}\left[\frac{R_{i,j}H_{i,j}^3}{\Delta R^2\overline{\mu}_{i,j}}+\frac{R_{i-1,j}H_{i-1,j}^3}{\overline{\mu}_{i-1,j}\Delta R^2}\right]$$
$$+P_{i,j+1}\left[\frac{H_{i,j}^3}{R_{i,j}\overline{\mu}_{i,j}\beta^2\Delta\overline{\theta}^2}+\frac{H_{i,j+1}^3}{R_{i,j}\overline{\mu}_{i,j+1}\beta^2\Delta\overline{\theta}^2}\right]$$
$$P_{i,j-1}\left[\frac{H_{i,j}^3}{R_{i,j}\overline{\mu}_{i,j}\beta^2\Delta\overline{\theta}^2}+\frac{H_{i,j-1}^3}{R_{i,j}\overline{\mu}_{i,j-1}\beta^2\Delta\overline{\theta}^2}\right]+P_{i,j}\left[-2\frac{R_{i,j}}{\Delta R^2}\frac{H_{i,j}^3}{\overline{\mu}_{i,j}}-\frac{R_{i+1,j}}{\overline{\mu}_{i+1,j}}\frac{H_{i+1,j}^3}{\Delta R^2}-\frac{R_{i-1,j}}{\overline{\mu}_{i-1,j}}\frac{H_{i-1,j}^3}{\Delta R^2}\right.$$
$$\left.-2\frac{H_{i,j}^3}{R_{i,j}\overline{\mu}_{i,j}\beta^2\Delta\overline{\theta}^2}-\frac{H_{i,j+1}^3}{R_{i,j}\overline{\mu}_{i,j+1}\beta^2\Delta\overline{\theta}^2}-\frac{H_{i,j-1}^3}{R_{i,j}\overline{\mu}_{i,j-1}\beta^2\Delta\overline{\theta}^2}\right]=\frac{6R_{i,j}}{\Delta\theta}\left[H_{i.j+1}-H_{i,j-1}\right]+12R_{i,j}\,\beta V \tag{10}$$

The calculation procedure uses these calculated pressures along with numerical methods for integration to obtain the load capacity , radial and angular location of centre of pressure. To ensure numerical accuracy the pressure distribution satisfied the 0.1 percent convergence limit.

4. DYNAMIC COEFFFICIENTS

a) The damping of the fluid film is its ability to absorb energy and is measured in N.sec/m. The damping coefficient, C_z , is calculated using

$$C_z=\frac{\Delta W}{\Delta V} \tag{11}$$

The subscript 'z' refers to the vertical direction of motion, orthogonal to the direction of the applied forces. Where W is the component of force causing displacement measured in N, and V is the vertical velocity measured in m/s. The formula for calculation of non-dimensional damping coefficient as in Storteig (1999) is

$$C_z{}^*=C_z\frac{U}{L}\left[\frac{h_{\min}{}^3}{BL^2U\mu eff}\right] \tag{12}$$

b) Similarly the stiffness of the fluid film is its ability to resist deformation by an applied force measured in N/m.

The stiffness coefficient, K_z, was calculated using

$$K_z = \frac{\Delta W}{\Delta h_o} \tag{13}$$

The formula for calculation of non-dimensional stiffness coefficient is

$$K_z{}^* = K_z \left[\frac{h_{\min}{}^3}{BL^2 U \mu eff} \right] \tag{14}$$

5. RESULTS AND DISCUSSIONS

Table 1 lists the bearing geometry, operating conditions and oil properties. Oil properties used in the software analysis did not correspond to those of the actual oils used in Ferguson(1998) but the influence of this inconsistency on the predictions was not significant. The present study aim's to supersede Vohr's analysis and determines the accuracy of the author's analysis by comparing it with that of Ettle's and Yuan (2001).

Table 1. Thrust Bearing Geometry

Outer Diameter (m)	1.168
Inner Diameter	0.711
Number of Pads	12
Thickness (mm)	30.2
Groove width (mm)	52.3
Number of Springs	12
Operating Conditions	
Load (MN)	2.124
Rotational speed (rads/s)	31.4
Oil pot temperature (º C)	70
Oil Properties	
ISO grade	32
$\gamma(cSt)$ at 40 º C	33.5
$\gamma(cSt)$ at 100 º C	5.45
$\rho(g/m)$ at 15 º C	0.868

Figure 5 shows the 3-dimensional pressure distribution obtained for the Mitchell's film shape and its model outlined in section 2.1. The pressure distribution near the trailing edge is

identical. Near the leading edge, however, the pressure at the outer radius is slightly less than the value for the Mitchell approximation. This is because of the lower oil film thickness for the Mitchell's model.

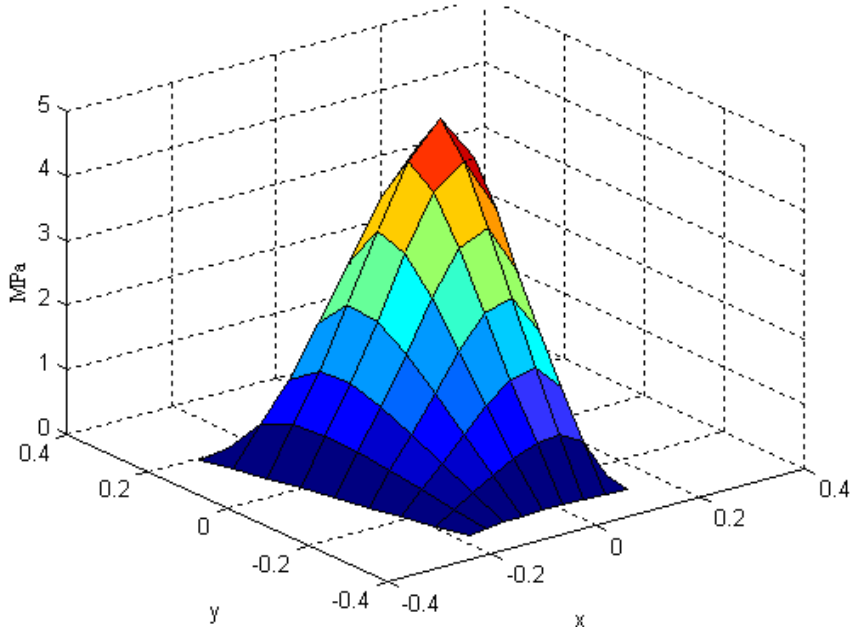

Figure 5. 3-D pressure distribution in the oil film of a flat pad.

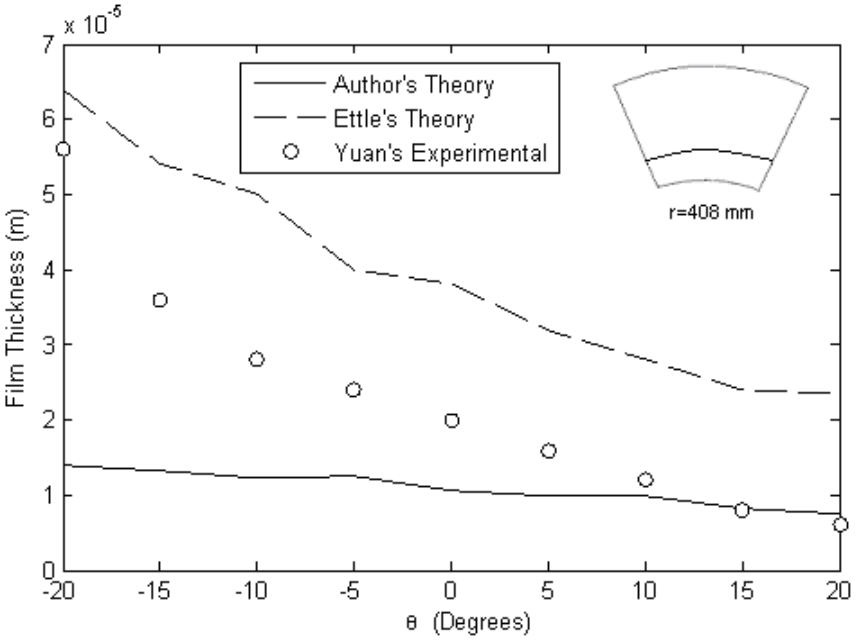

Figure 6(a). Theoretical and Experimental film thickness at r=408mm.

The agreement between film thickness is related to the agreements for pressures the author's, Ettle's and Yuan's predictions. A comparison of the film thickness values showed poor agreement as in Figures 6.a-.d.

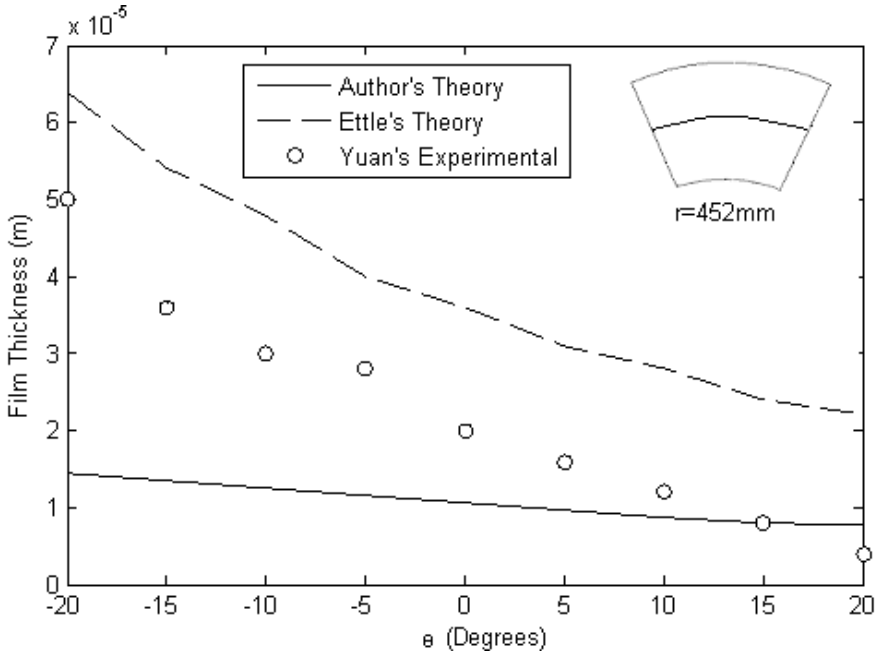

Figure 6(b).Theoretical and Experimental film thickness at r=452 mm.

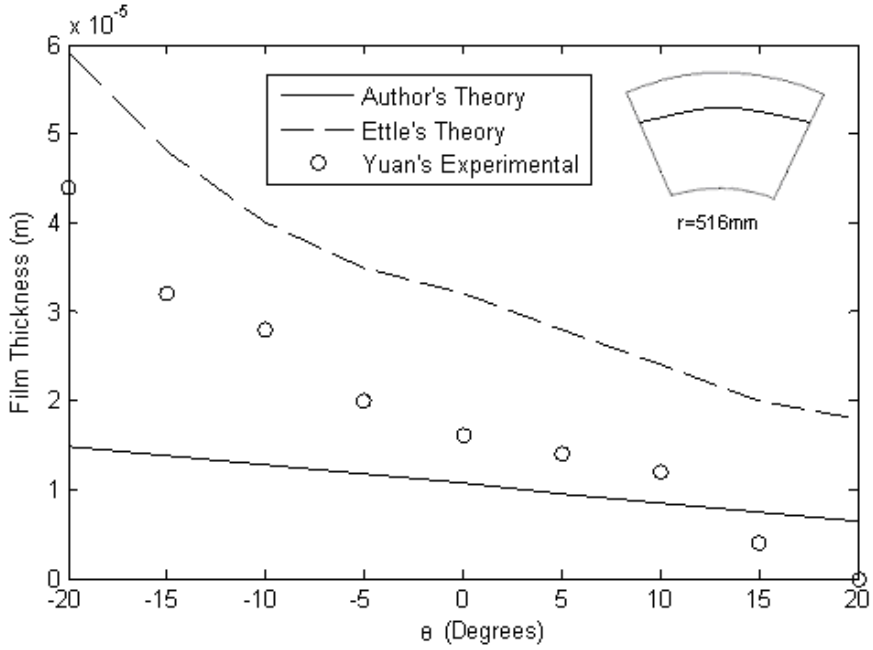

Figure 6(c). Theoretical and Experimental film thickness at r=516 mm.

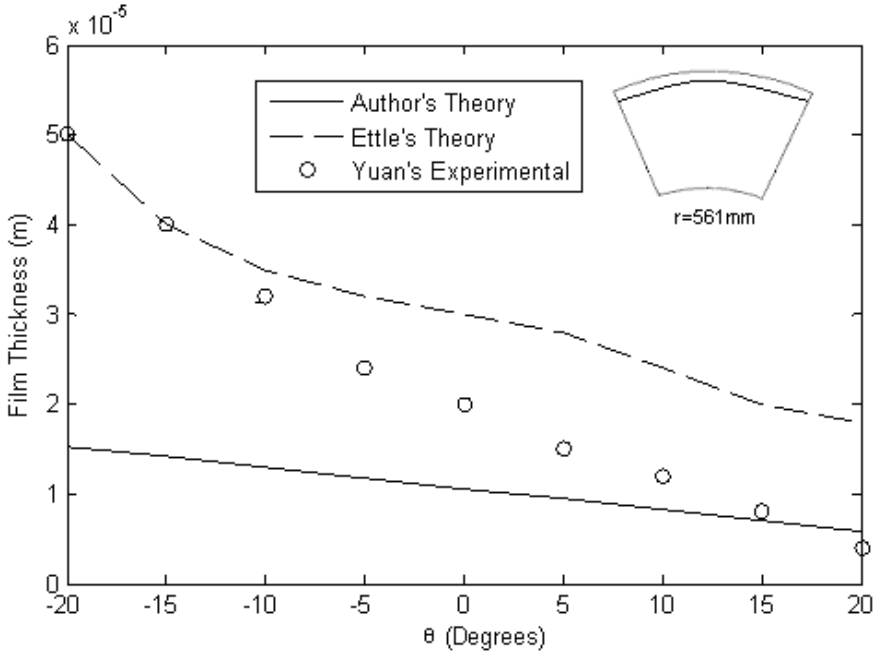

Figure 6(d). Theoretical and Experimental film thickness at r=561mm.

The system had some inherent filtering and further manual filtering from taking average discrete values by hand from the plots on the chart recorder. The overall precision of the film thickness values for both the theoretical and experimental values was estimated at about ± 4 μm. Large hydroelectric generators are usually designed as vertical axis machines with the generator above a hydraulic turbine. The rotating parts and hydraulic load are supported by a thrust bearing.

The uncertainty in the film thickness measurements could not be quantified but it was suggested that the pad shape had been measured with quite good fidelity. The comparison of Yuan's experimental, Ettle's theoretical and present solution results supported this suggestion. Except for probe 4 (Figure 6.d.), which passed over the outer edge of the pads, to give the same values as the present solution over the inlet half of the pad, the other probes consistently underestimated the film thickness.. The software packages might have given a reduced film thickness in this region because of poor choices of heat transfer coefficients or imprecision in the thermo elastic deflection modeling which just happened to correspond to the experimental results which were low because of the problem of measuring an accurate probe voltage at zero film thickness.

Unfortunately, theory predicted much smaller pressures in the central region of the pad than were measured in the experiments (Figure 7). The accuracy of the pressure measurements had been estimated at about ± 0.2 MPa.

The small uncertainty range suggested that the fairly large differences between the experimental data and the predictions of the author's and Ettle's software program's were attributable to inaccuracies in the theoretical modeling. The input data used for calculation of damping and stiffness coefficients in the tilting – pad thrust bearing was $D_O = 1.275m; D_i = 0.75m; z = 6; G_p = 0.084;\ \omega = 14.28 rad/\sec;\ h_o = 52.5e-6m;$

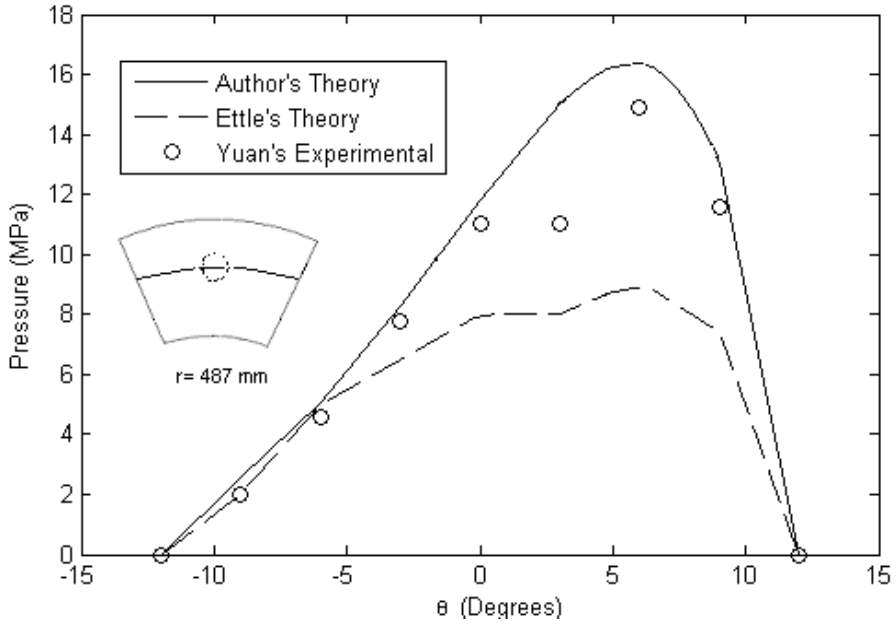

Figure 7(a). Theoretical and Experimental Pressures along the $R_{cp.}$

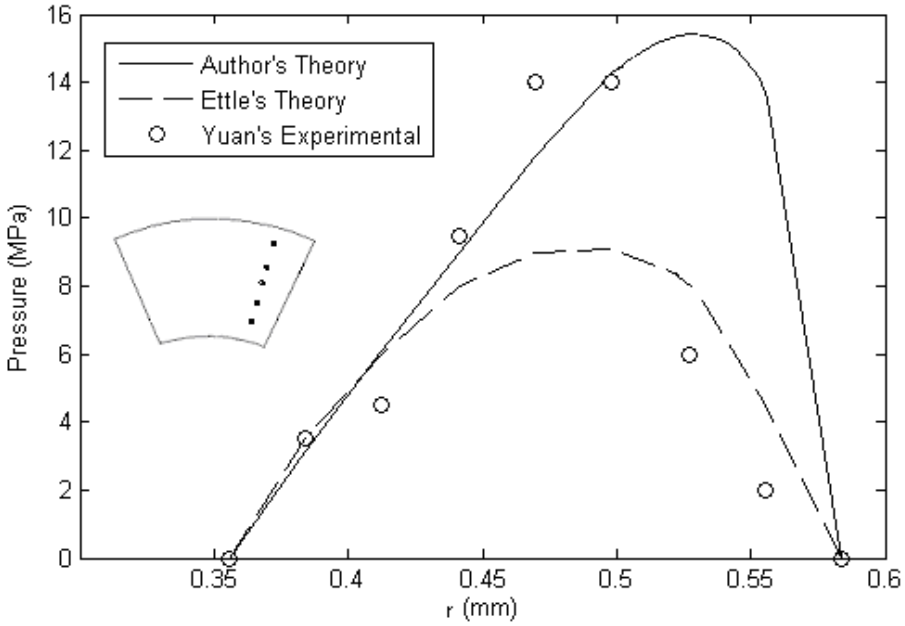

Figure 7(b). Theoretical and Experimental Pressures from R_i to $R_{o.}$

Initially we gradient film thickness coefficients by substituting the values of a and h_o in the equation for the oil film shape. By substituting these gradient film thicknesses in modified Reynold's equation we get pressure at each node. Numerical integration to these pressure points gives the load.

V and h_o values are varied from +10% to -10% and the change in values of W so obtained is denoted as ΔW . Based on these values dimensional and non-dimensional damping and stiffness coefficients are calculated in Table 2. and Table 3. respectively, for the author's dimensional parameters considering L/B = 0.7 and a=1.

Table 2. Values of 'C_z' Corresponding to 'ΔW' and 'ΔV'

	± 2%	± 4%	± 6%	± 8%	± 10%
ΔW	263.8	425.6	796.6	1068.2	1616.7
ΔV	.293e-4	.594e-4	.89e-4	1.49e-4	1.49e-4
C_z	888e4	716e4	894e4	717e4	1088e4
C_z^*	1.4*10-8	3*10-8	3.7*10-8	3*10-8	4.5*10-8

Table 3. Values of $'K_z'$ corresponding to $'\Delta W'$ and $'\Delta h_o'$

	± 2%	±4%	±6%	±8%	±10%
ΔW	263.8	425.6	796.6	1068.2	1616.7
Δh_o	.0052	.0104	.0156	.0208	.0260
K_z	50678	40880	51011	51302	62116
K_z^*	5.0*10-9	4.0*10-9	5.0*10-9	5.0*10-9	6.1*10-9

Figure 8 and Figure 9 show non-dimensional damping and stiffness coefficient contour plots respectively for 'a' varied from 1.0 to 2.2 and L/B from 0.7 to 1.3.

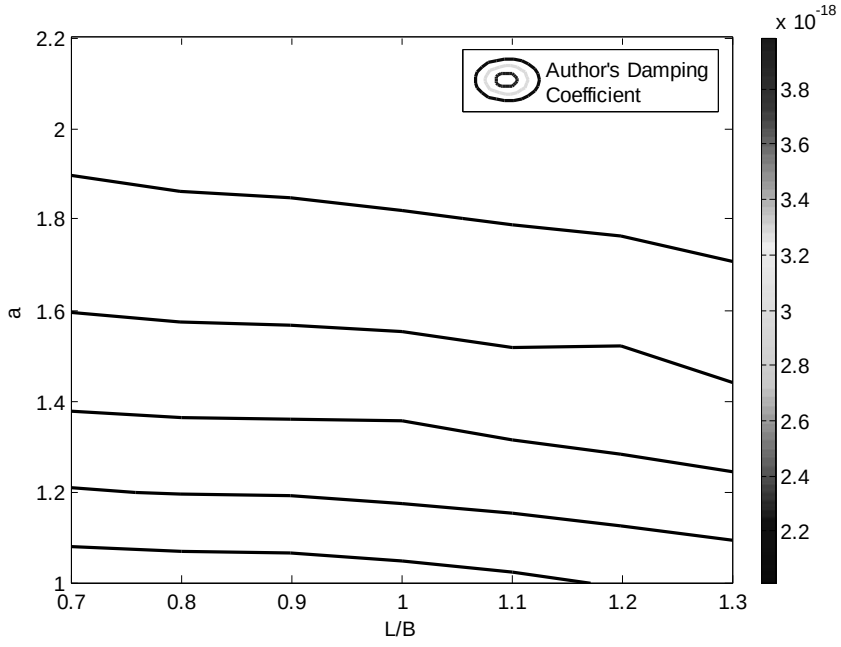

Figure 8. Non-dimensional damping C_z with respect to film shape parameter *a* and *L/B* ratio.

The author's non-dimensional damping coefficient value at L/B = 0.7 and a=1 is 4.3114e-18 and decreases gradually as 'a' and L/B are increased and finally at a = 2.2 and L/B = 1.3 the value becomes 1.5006e-18. The value of the non-dimensional stiffness coefficient at L/B = 0.7 and 'a' = 1.0 is 1.6006e-20 and increases gradually and at 'a'= 2.2 and L/B = 1.3 is equal to 4.5713e-21.

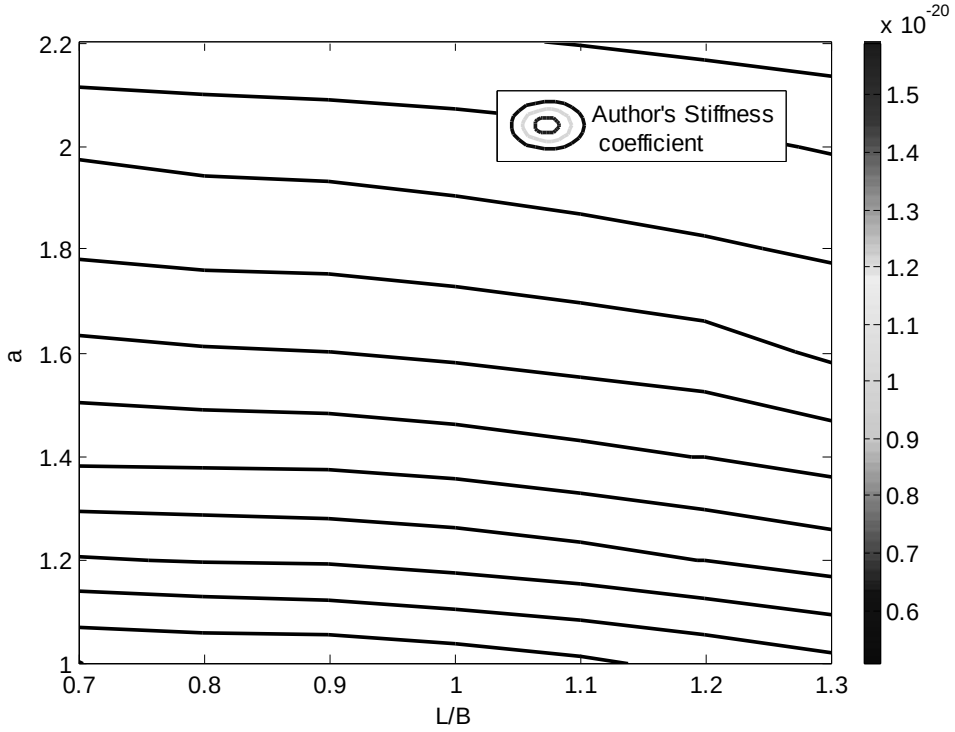

Figure 9. Non-dimensional stiffness K_z with respect to film shape parameter *a* and *L/B* ratio.

CONCLUSIONS

Formulation of the oil film shape and variation of film thickness along and across the flat sector pad surface is done. Two dimensional Reynold's equation is modified and a finite difference method based solution procedure for finding pressure values is written and verified. Numerical integration to these pressure points gives the load. The software packages might have given a reduced film thickness in this region because of poor choices of heat transfer coefficients or imprecision in the thermo elastic deflection modeling. The differences in experimental and present solution pressures might have been caused by rotor crowning giving thicker films than predicted by theory at the outer edge of the bearing. Additional factors are imprecise thermal boundary conditions and inaccuracies in the thermo elastic deflection model within the software packages.

Agreement between theoretical and experimental results although not perfect did provide solid support for the utility of the software package in predicting large spring-supported thrust bearing behaviour. The agreement for pressures was not as good but the theoretical pressure

distribution was likely to be very sensitive to slight inaccuracies of the film thickness and more specifically the pad shape in the theoretical modeling. The fixed error of unknown extent from the determination of the voltage equivalent to zero film thickness made the comparison of present solution, Ettle's theoretical and Yuan's experimental film thicknesses qualitative in nature. Subsequently the non-dimensional damping and stiffness coefficients for the variation of film thickness and introduction of vertical velocity were determined. This data is useful as an input for rotor dynamic studies of the vertical rotors Future work should include reducing experimental uncertainity ranges and modifying the experiments both to simulate further specific features of large spring-supported thrust bearings in service and to test the modeling assumptions of the software package more rigorously.

REFERENCES

Cameroon, A., (1966), "*Principles of Lubrication*", Longmans , London.

Capitao,J.W,(1974), "Influence of Turbulence on Performance Characteristics of the Tilting Pad Thrust Bearing", Transactions of the ASME, *Journal of Lubrication Technology,* January,pp.110-117.

Chaturvedi , K.K., Athre, K., Nath,Y. and Biswas ,S., (1989), "Refinement in Estimation of Load Capacity and Temperature Distribution of Pad Bearing," *Proceedings of Eurotrib*-89, Helisinki, Finland , June.

Eskild Storteig, Maurice F. White, (1999) , "Dynamic Characteristics of Hydro-dynamically Lubricated Fixed-Pad Thrust Bearings", *Wear,* vol.232, pp.250-255.

Etsion, I., (1978) , "Design Charts for Arbitrarily – Pivoted, Liquid Lubricated, Flat Sector-Pad Thrust Bearing", Journal of Lubrication Technology, *Transactions of the ASME*, vol. 100, April , pp.279-286.

Ettles, C., (1991), "Some Factors Affecting the Design of Spring Supported Thrust Bearings in Hydroelectric Generators", *Journal of Tribology, Trans. of the ASME*, vol.113, no.6, July, pp.626-632.

Ettles, C.M.M. and Anderson , H.G., (1991), " Three – Dimensional Thermo - Elastic solutions of Thrust Bearings using code Marmac 1", *Journal of Tribology, Transactions of the ASME*, vol. 112, pp. 405- 412.

Pinkus, O, and Sternlicht, B., (1961), "*Theory of Hydrodynamic Lubrication*", Mc Graw Hill.

Vohr., J.H, (1981), "Prediction of the Operating Temperature of Thrust Bearings", ASME, *Journal of Lubrication technology*, 103, pp 97-106.

Yuan J.H., Ferguson J.H. and Medley J.B., (1998), "Spring Supported Thrust Bearings for Hydroelectric Generators: Influence of oil viscosity on power loss", *Proceedings Energy Conservation in Trib*. Series , 24. Elsevier, pp.187-194.

Yuan J.H., Ferguson J.H. and Medley J.B., (1999), "Spring Supported Thrust Bearings used in Hydroelectric Generators: Labratory testing facility", *STLE Tribology Transactions*, January, pp.126-135.

Yuan J.H., Ferguson J.H. and Medley J.B., (2001), "Spring Supported Thrust Bearings Hydroelectric Generators: Comparison of Experimental Data with Numerical Predictions", *STLE Tribology Transactions*, vol. 44 , pp.27-34.